ADVANCES IN ATMOSPHERIC SCIENCES, VOL. 25, NO. 2, 2008, 213–226

Simulating the Effects of the 1991 Mount Pinatubo Volcanic Eruption Using the ARPEGE Atmosphere General Circulation Model

Odd Helge OTTERÅ*[1,2]

[1]*Nansen Environmental and Remote Sensing Center, Thormøhlensgt.* 47, 5006 *Bergen, Norway*

[2]*Bjerknes Centre for Climate Research, Allégt.* 55, 5007 *Bergen, Norway*

(Received 8 January 2006; revised 30 April 2007)

ABSTRACT

The climate changes that occured following the volcanic eruption of Mount Pinatubo in the Phillippines on 15 June 1991 have been simulated using the ARPEGE atmosphere general circulation model (AGCM). The model was forced by a reconstructed spatial-time distribution of stratospheric aerosols intended for use in long climate simulations. Four statistical ensembles of the AGCM simulations with and without volcanic aerosols over a period of 5 years following the eruption have been made, and the calculated fields have been compared to available observations. The model is able to reproduce some of the observed features after the eruption, such as the winter warming pattern that was observed over the Northern Hemisphere (NH) during the following winters. This pattern was caused by an enhanced Equator-to-pole temperature gradient in the stratosphere that developed due to aerosol heating of the tropics. This in turn led to a strengthening of the polar vortex, which tends to modulate the planetary wave field in such a way that an anomalously positive Arctic Oscillation pattern is produced in the troposphere and at the surface, favouring warm conditions over the NH. During the summer, the model produced a more uniform cooling over the NH.

Key words: volcanic aerosol, climate, Mount Pinatubo, Arctic Oscillation

DOI: 10.1007/s00376-008-0213-3

1. Introduction

There has been considerable debate as to the role that humans have played in changing global climate through the burning of fossil fuels and the release of chlorofluorocarbon (CFC) gases. However, attribution of any observed climatic change to anthropogenic forcing is complicated by the fact that human-induced changes will be superimposed on the natural climate variability observed. Volcanic eruptions are an important cause of weather and climate change over many different time scales ranging from hours to decades (Robock, 2000), so understanding the role of volcanic eruptions (and other natural processes) on the global climate system is important to understand the ongoing climate change debate more completely.

Explosive volcanic eruptions inject a large amount of different types of particles and gases, such as water vapor (H_2O), carbon dioxide (CO_2), sulfur dioxide (SO_2), chlorine (Cl^-), fluorine (F^-) and ash, into the stratosphere. Most of the ash is washed out of the atmosphere quite rapidly, on timescales of minutes to a few weeks in the troposphere. Small amounts can last for a few months in the stratosphere, but the climatic impact is negligible. Gases such as H_2O and CO_2 are important greenhouse gases, but their atmospheric concentrations are so large that individual eruptions have a minimal effect upon the overall concentrations, and thus do not directly impact the greenhouse effect. The most important climatic effect of these explosive volcanic eruptions is rather through the emission of sulphur species, mostly as SO_2, into the stratosphere. The SO_2 is then rapidly converted into sulphuric acid (H_2SO_4), which in turn condenses into aerosols. These stratospheric aerosols reflect the radiation from the Sun, thus cooling the troposphere. Furthermore, these stratospheric aerosols can also absorb both solar near-infrared and outgoing longwave

*Corresponding author: Odd Helge OTTERÅ, oddho@nersc.no

(LW) radiation, which in turn will lead to a warming of the stratosphere. Finally, the stratospheric aerosols can also lead to ozone destruction by altering chlorine and nitrogen chemical species in the stratosphere (e.g., Sato et al., 1993; Solomon et al., 1998). A more thorough and comprehensive review of the relationships between explosive volcanic eruptions and climate can be found in Robock (2000).

Currently, numerical models such as general circulation (GCMs) and state-of-the-art climate models are the best tools available for providing predictions of future climate change. However, in order to increase our confidence in these models as accurate predictors of future climate change, it is important that they are able to simulate as realistically as possible a wide range of different atmosphere and atmosphere-ocean variabilities, including the climate effects due to volcanic eruptions. Furthermore, climate reconstructions of the last millennium have received a lot of attention in recent years (e.g., Mann et al., 1999; Briffa et al., 2001; Esper et al., 2002; Jones and Mann, 2004) with the ultimate goal of estimating the level of natural variability in the absence of large anthropogenic influences. Transient climate simulations, with state-of-the-art climate models, contribute to the clarification of some of the discrepancies between some of these climate reconstructions that have been presented so far, and can also help to identify the mechanisms that may lead to an amplification or reduction of the effects of the varying external forcings. In order for such long transient simulations to be successful, reliable records of all relevant external forcings, including volcanic aerosol loading into the atmosphere, are needed.

Over the last few decades or so, a number of volcanic indices have been generated, most of which having significant deficiencies. A perfect volcanic index would ideally describe the radiative forcing associated with each volcanic eruption. The radiative forcing is mostly associated with the sulphur content of the various emissions that reach the stratosphere and not those associated with the explosiveness of the eruption. Unfortunately, all indirect volcanic indices are either incomplete in geographical or temporal coverage, or provide a measure of a property of volcanic eruptions other than their stratospheric aerosol loading. The best technique currently available is probably direct radiation measurements, and combinations of surface, aircraft, balloon, and satellite measurements have contributed to better quantifying the distribution and optical properties of the aerosols from recent volcanic eruptions such as the 1982 El Chicón (Robock, 1983) and 1991 Mount Pinatubo (Stenchikov et al., 1998). For past climates, geological methods based on the examination of sulphate deposition in ice cores at Greenland and Antarctica has been used to estimate sulphate forcing back through the Holocene (Hammer et al., 1997; Udisti et al., 2000). The most reliable records are from the last 1000 years or so (Crowley, 2000; Robertson et al., 2001) and these are also most commonly used in long transient climate simulations (e.g., Zorita et al., 2004; Stendel et al., 2006).

The 15 June 1991 Mount Pinatubo eruption was a large, but relatively short-lived, shock to the Earth's atmosphere. The eruption produced the largest sulphur oxide cloud that occured in the 20th century. The combined aerosol plume of Mount Pinatubo diffused around the globe in a matter of months. The data collected after this eruption showed that the mean world temperatures decreased by about 0.5°C over the subsequent two years. The eruption provided an excellent opportunity to study the important processes of the climate system in more details, and furthermore provided a possibility to test the various climate models available. For instance, Soden et al. (2002) used the global cooling and drying of the atmosphere that was observed after the Pinatubo eruption to test climate model predictions of the climate feedback from water vapour. The results provided quantitative evidence of the reliability of water vapour feedback in climate models, which is important to their use for global warming projections.

A somewhat surprising finding after the Mount Pinatubo eruption, was the observed winter warming over the NH continents in the following two winters after the eruption. This warming, which is common for most large tropical volcanic eruptions, is now understood as a dynamical response to the radiative perturbation from the volcanic aerosols, as well as the ozone depletion that occured following the eruption. This winter warming phenomenon is characterized by a positive mode of the Arctic Oscillation (AO; Thompson and Wallace, 1998), which can be produced by an enhanced temperature gradient in the lower stratosphere due to the aerosol heating occuring in the tropics. Several observational (Groisman, 1992; Robock and Mao, 1995) and modelling (Kirchner et al., 1999; Stenchikov et al., 2002; Shindell et al., 2004) studies have tended to support this finding.

In the study reported here, the implementation of volcanic aerosols into the atmospheric general circulation model ARPEGE is described, and results from a simulation using this model of the largest volcanic eruption of the 20th century, the Mount Pinatubo eruption of 1991, are presented. The goal was to determine the extent the model was able to reproduce some of the main observed features after this eruption. The study focused particularly on the atmospheric mechanism of the AO response to volcanic forcing that pre-

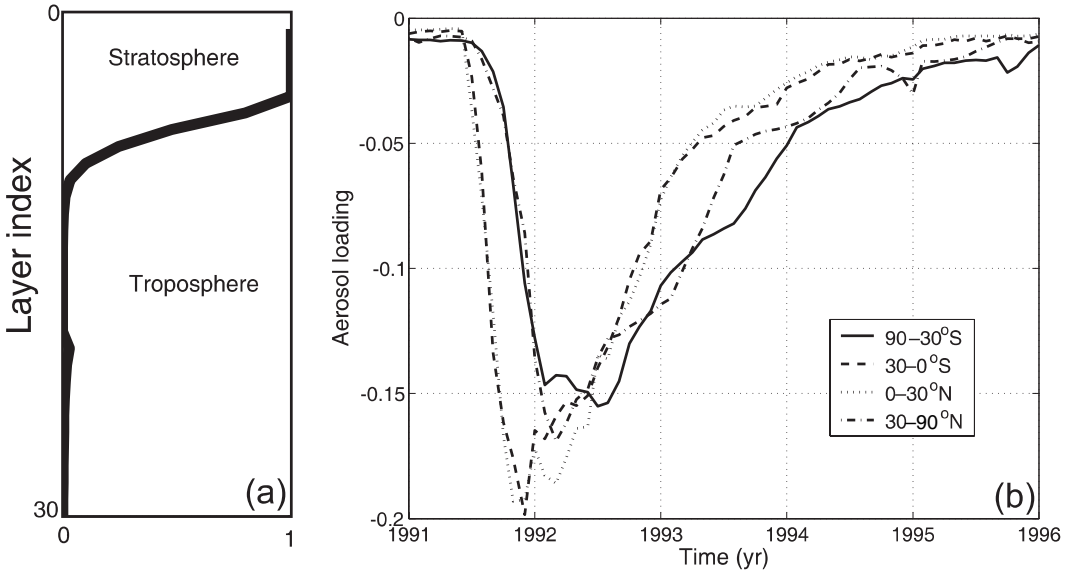

Fig. 1. (a) Vertical distribution of the aerosol loading in ARPEGE. (b) Aerosol loading (optical depth at 0.55 μm) between 1991 and 1996, based on updated data from Crowley et al. (2003).

sumably played a dominant role on the shorter timescales lasting from a season up to a year. This study only deals with the radiative effects of the Mount Pinatubo eruption. Other potentially important factors, such as ozone depletion, the quasi-biennial cycle and the impact of inter-annual sea surface temperature (SST) variations, have not been included.

The paper is organized as follows: In section 2 the atmosphere model is described, the procedure for including volcanic (stratospheric) aerosols into the model is outlined, and the set-up of the experiment is provided. The results are presented in section 3. Finally, the results are discussed and summarized in section 4.

2. Experimental design

The atmospheric model is the spectral AGCM model ARPEGE/IFS from METRO FRANCE (Déqué et al., 1994). In the present study, ARPEGE/IFS was run with a truncation at wave number 63 (T_L63), and a time step of 1800 s. The linear T_L63 grid has the same number of points as the quadratic T42 grid, with a horizontal resolution of about 2.8° × 2.8°. A total of 31 vertical levels are employed, with 21 in the troposphere and 10 in the stratosphere. More details regarding the model description and the physical parameterization schemes can be found in Furevik et al. (2003).

The aerosol climatology that has been used in ARPEGE included a total of five different types of aerosols: continental, maritime, urban, desert and stratospheric aerosols. The horizontal distribution of the first four was proposed by Tanre et al. (1984), while the stratospheric background aerosols were uniformly distributed on the sphere. The vertical distribution is described by an exponential decrease with increasing height and has a smooth overlapping between the stratosphere and the troposphere through a weighting function (Fig. 1a). The optical properties of the five aerosol types were calculated from the aerosol model of WMO-ICSU (1984). Hu et al. (2001) have introduced a sixth type, sulphate aerosols. The horizontal distribution for this type was provided by Penner et al. (1998) and the vertical distribution was obtained from Chin et al. (1996).

In this study, an updated version of the time series of Crowley et al. (2003) was used for volcanic aerosols, including the effects of the Mount Pinatubo eruption (out to 1999, by applying a decay time of 1 year, consistent with observations). The time series was supplied as monthly optical depths at 0.55 microns, in the middle of the visible spectrum. These were applied in ARPEGE as quarterspheric (30°–90°N, 0°–30°N, 30°S–0°, 90°–30°S) monthly values (Fig. 1b). The aerosol was then distributed in each model level in the stratosphere. The volcanic mass of the stratospheric aerosols were calculated at each grid-point and model level in the stratosphere by dividing the total aerosol concentration by the total air mass of all stratospheric levels at that grid point.

For this study, four pairs of 5-year model integrations were performed, each starting in January, 1991 (5 months before the Mount Pinatubo eruption). Each

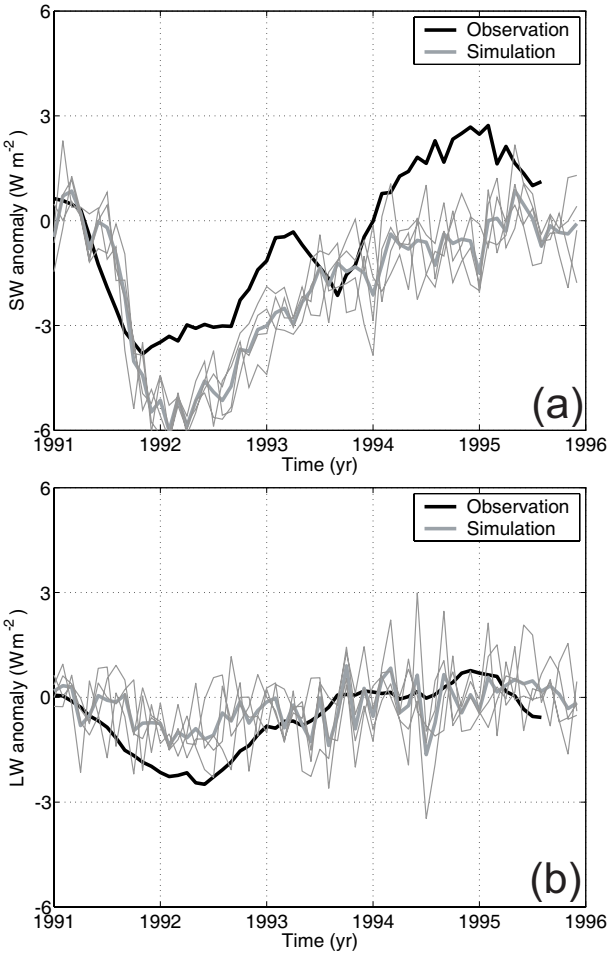

Fig. 2. Comparison of the observed anomalies in the (a) absorbed SW and (b) emitted LW radiative fluxes located at the top of the atmosphere from the Earth Radiation Budget Satellite observations (thick black line, which is the 7-month running mean) and four ensembles of GCM simulations (grey lines; thick grey line is the ensemble mean). The observed anomalies are expressed relative to a 1985 to 1990 base climatology.

experimental pair consisted of a control simulation, in which no stratospheric aerosols were used, and a Mount Pinatubo simulation, in which the model was perturbed using the updated volcanic aerosol time series of Crowley et al. (2003) for the period from 1991 to 1996. The model was run with modern day vegetation, topography, insolation and modern levels of greenhouse gases and tropospheric aerosols. All integrations were forced with monthly climatological SST and sea-ice according to Reynolds and Smith (1995).

The experiments were restarted with different initial conditions (same for corresponding experiments with and without stratospheric aerosols). The different initial conditions were generated in a prior fifteen-day simulation using the daily output of a history restart file at a specified time of day. Due to the highly chaotic nature of the atmospheric model, each realization is statistically independent after a short period of integration (e.g., Lorenz, 1968). The results have been evaluated by averaging the meteorological fields over the ensembles of the control simulations and the Mount Pinatubo simulations (hereafter referred to as the CO and MP simulations, respectively), and calculating the statistical significance using a local t-test.

3. Results

The surface air temperature (SAT) was chosen to characterize the climatic effects of the eruption, while analysis of the sea level pressure (SLP) and geopotential heights were chosen to describe the general circulation response. The model results were compared with different observational evidence to see whether or not the model was consistent. For SAT, SLP and geopotential height, the gridded reanalysis data from the National Centers of Environmental Prediction (NCEP, Kalnay et al., 1996) were used. In addition, the time series of the globally-averaged SAT, compiled by the Climate Research Unit (CRU) and the UK Meteorological Office Hadley Centre (Jones et al., 1999; Jones and Moberg, 2003), was also used. The simulated radiative flux anomalies were compared with the radiative fluxes at the top of the atmosphere provided by the Earth Radiation Budget Satellite (ERBS) observations.

3.1 *Response of the radiative fluxes*

The change in the radiative fluxes at the top of the atmosphere characterizes the change in the energy input into the whole climate system (Fig. 2). Both the observations and the model simulations provided similar reductions in the absorbed shortwave (SW) radiation (Fig. 2a). In the observations, the reduction of the solar energy reached its largest value of more than 4 W m^{-2} during the first winter after the eruption, while the maximum reduction in the model simulations was slightly larger (about 6 W m^{-2}). On the other hand, the simulated LW radiation reduction was weaker than in the observations, with about a 1.5 W m^{-2} reduction in the model, compared to the 2 W m^{-2} reported in the ERBS data (Fig. 2b). The net solar SW flux reduction was not compensated by the LW aerosol absorption, making the total radiative forcing negative. The SW+LW net flux anomaly reached a maximum reduction of about 4.5 W m^{-2} in January, 1992. This was on the high end of the values reported by Minnis et al. (1993) using the ERBS data (-2.7 ± 1 W m^{-2}), and Shindell et al. (2004) obtained from optical measurements (-3.73 W m^{-2}).

The global average radiation balance correlates

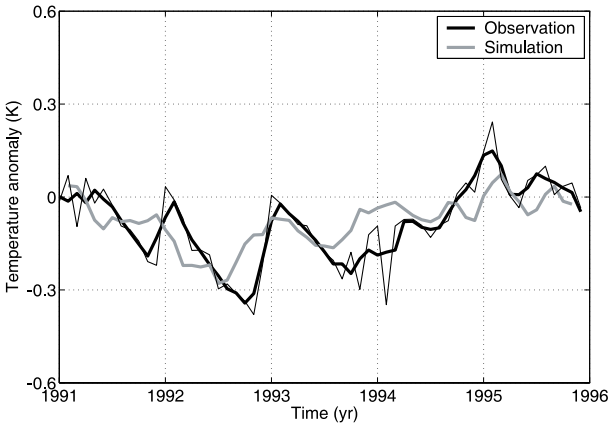

Fig. 3. Simulated (grey line) and observed (thick black line, which is the three-month running mean; thin line is the unfiltered time series) globally-averaged air-temperature anomalies from 1991 to 1996. The observations were taken from Jones et al. (1999).

well with the evolution of the aerosol optical depth (Fig. 1b), and the differences between all four ensemble members were substantially smaller than the forcing itself. From 1994 onwards, positive anomalies in the SW radiation fluxes were found in the observations. These anomalies were unrelated to the Mount Pinatubo eruption and therefore not reproduced in the model simulations. These anomalies are believed to have originated from decadal-scale changes in the tropical circulation during the mid- to late 1990s (Chen et al., 2002; Wielicki et al., 2002).

3.2 *Surface air temperature response*

The simulated globally averaged SAT anomaly agreed well with the observations from CRU (Fig. 3). This cooling reached its maximum in July of the year after the eruption, with a cooling of around 0.3 degrees. The timing of the maximum cooling was somewhat earlier (about 2 months) when compared with the observations. During the winter, the amplitude of the temperature anomaly was decreased in the observations, as well as in the simulations, due to the winter warming effect that occured in the NH. This winter warming phenomenon is now quite well understood as a dynamical response of the climate system to the radiative forcing, and is closely related to tropospheric and stratospheric circulation changes (see below).

Figure 4 shows the simulated and observed patterns of SAT anomalies in the first winter after the Mount Pinatubo eruption. The observed temperature anomaly patterns from the NCEP reanalysis were calculated relative to the period 1985–1990. The 1985–1990 baseline climatological period was chosen so as to exclude the possible influence of the 1982 El Chicón eruption and ensured that the period was short enough so that long-term trends were not important. The observed temperature anomaly patterns from the NCEP reanalysis (Fig. 4a) were similar to the mean SAT anomalies calculated for the many large tropical eruptions that occured over the last 400 years (Shindell et al., 2004). The observed winter patterns following these large tropical eruptions were typically characterized by a broad warming over northern Eurasia and Europe, as well as over much of the United States. Significant cold anomalies were typically located over Greenland and parts of Alaska, the Middle East and China. The simulated winter pattern agreed reasonably well with this pattern (Fig. 4b). The most significant warm anomalies were found over Eurasia, while the warming over Europe was weaker than in the observations. Furthermore, the warming that occured over North America was located further to the north than in the observations. The cold anomalies that were observed over Labrador, the Middle East and China were well captured by the model.

In the summer, the observations showed a general cooling over the landmasses in the NH, except for over the areas over Europe, where the reanalysis data showed a warming (Fig. 5a). This warming was not reproduced by the model, which instead showed a significant cooling over this region (Fig. 5b). Elsewhere, the simulated cooling over the North American continent was too weak when compared to the observations, while the cooling over Greenland and the Barents region, as well as over parts of Russia, agreed better with the observations. The model also failed to reproduce an observed cooling that occured over China. This difference was not unexpected, as some previous studies have shown that decadal variability, which is not resolved in the simulations, partly dominates this observed cooling (Hu et al., 2003; Yu et al., 2004).

3.3 *Sea level pressure response*

The winter high-latitude warming observed in both the observations as well as in the model simulations have been shown to be consistent with an increased westerly circulation in the NH that are associated with a positive shift in the mean state of the AO (e.g., Groisman, 1992; Robock and Mao, 1995; Kirchner et al., 1999; Stenchikov et al., 2002; Shindell et al., 2004). This favours stronger westerlies and a more northerly storm-track across the Atlantic, bringing warm, moist air to Northern Europe and Russia, and cold, dry air to regions around the Mediterranean basin. The AO, formally defined as the first hemispheric empirical orthogonal function of SLP variability (Thompson and Wallace, 1998), resembles the North Atlantic Oscillation (NAO; Hurrell, 1995) in many respects, but its

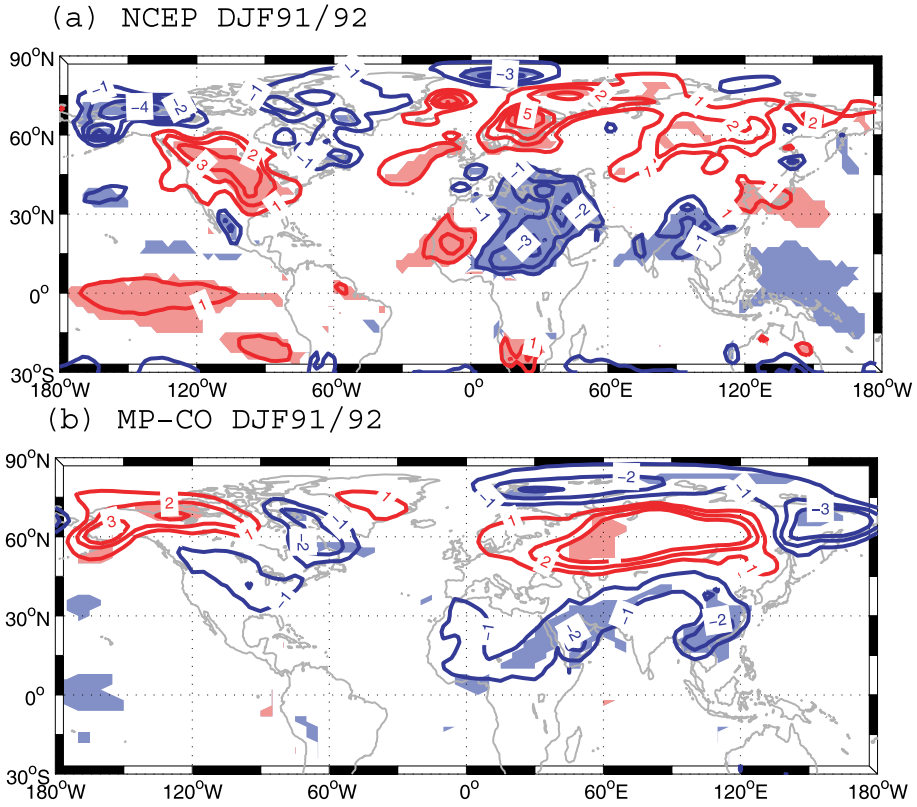

Fig. 4. Comparison of (a) the observed and (b) the simulated 1991/92 winter (DJF) temperature anomalies. The observed anomalies were calculated from a 1985 to 1990 base climatology. The simulated anomalies were calculated as the difference between the ensemble mean of the two pairs of simulations (MP−CO). Positive anomalies are shown in red. The shading indicates (a) anomalies exceeding one standard deviation, where the standard deviation was calculated using winter-mean quantities for the period 1951–1990, and (b) the 90 % confidence level based on a local t-test.

primary centre of action covers more of the Arctic, giving it a more zonally symmetrical appearance. The observations showed a strong, low pressure anomaly that was centred over the Arctic, extending southwards into Eurasia (Fig. 6a). This high-latitude, negative SLP anomaly was mostly surrounded by positive SLP anomalies in the mid-latitudes, but this was most pronounced in the regions located over the Atlantic sector and the Mediterranean. The strong meridional SLP gradient in the Atlantic sector drove the westerly surface-wind anomalies that helped to account for the corresponding warm surface anomalies observed in northern Europe and Eurasia (Fig. 4a). In the north Pacific, a negative anomaly was seen, which was most likely linked to Pacific SST variability.

The simulated SLP response showed a similar basic pattern (excluding the North Pacific) of low pressure over the pole, and was surrounded by a ring of anomalously high pressure (Fig. 6b). However, the simulated Atlantic dipole pattern was much weaker than in the observations due to an underestimation of the Azores maxima in the model. The simulated pattern had a more zonally symmetric appearance than in the observations and beared some resemblance to a positive phase of the AO (Thompson and Wallace, 1998).

3.4 *Stratospheric and mid-troposphere circulation response*

It has long been known that the stratosphere is heated following the injection of stratospheric aerosols after large volcanic eruptions (e.g., Quiroz, 1983; Parker and Brownscombe, 1983; Angell, 1997). This heating is caused by the absorption of both near-infrared solar radiation at the top and LW radiation at the bottom of the layer. Figure 7 shows the temporal evolution of the zonally averaged (observed and simulated) stratospheric temperature anomaly at the 50 hPa level. According to the NCEP reanalysis data the zonal-mean temperature anomaly in the lower stratosphere at 50 hPa showed a relatively complex spatial-

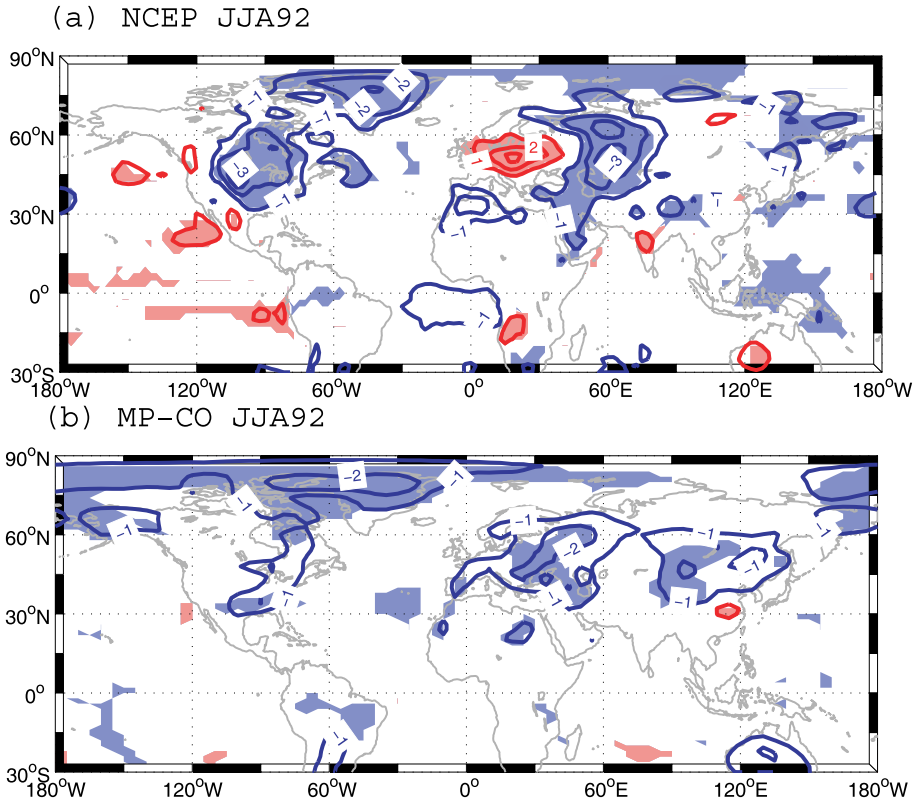

Fig. 5. Comparison of (a) the observed and (b) the simulated 1992 summer (JJA) temperature anomalies. The observed anomalies were calculated from a 1985 to 1990 base climatology. The simulated anomalies were calculated as the difference between the ensemble mean of the two pairs of simulations (MP−CO). Positive anomalies are shown in red. The shading indicates (a) anomalies exceeding one standard deviation, where the standard deviation was calculated using winter-mean quantities for the period 1951–1990, and (b) the 90% confidence level based on a local *t*-test.

temporal structure (Fig. 7a). In the winter and spring of 1992, the strongest warming (about 2–3 K) was observed at 30°N. In the summer of 1992, the tropical temperature anomaly was strongly reduced, while the positive anomalies reappeared in the tropics during the winter of 1992/93. The model simulated a strong tropical heating that was in excess of 4 degrees during the first winter after the eruption (Fig. 7b). This warming was more than twice as large as the observed warming in the NCEP reanalysis data set. This warming gradually diminished during the summer of 1992. In the winter of 1992/93, the simulated stratospheric warming was about 2 K and was similar to the observed warming. The reason for the relatively large discrepancies between the calculated aerosol effect and the observations are most likely related to the quasi-biennial oscillation and ozone depletion, which both contributed to the observed response (Kirchner et al., 1999; Yang and Schlesinger, 2002).

Figure 8 presents the changes in the zonally-averaged zonal-winter circulation. In the CO simulations, there are two main jet streams at the polar latitudes, one in each hemisphere (Fig. 8a). In the troposphere, the centres of action were found just below the tropopause at about 200 hPa and were located around 30°–40°N for the NH, and around 40°–50°S for the southern hemisphere. The stratosphere is characterized by an easterly jet that extends across the Equator, and a westerly jet (winter-polar vortex) in the northern high latitudes, with a centre of action at about 50°N. In the MP simulations, the winter of 1991/92 was characterized by a relatively strong increase (about 4 m s^{-1}) in the zonal wind in the stratosphere to the north of approximately 60°N, indicating a strengthening and a poleward shift of the polar vortex (Fig. 8b). In the troposphere, the centre of action for the westerly jet was actually somewhat reduced, while a significant increase in the zonal wind were found further to the north (around 60°N) extending through the entire troposphere, indicating a slight strengthening and a poleward shift of the jet.

The changes in the polar vortex were closely related

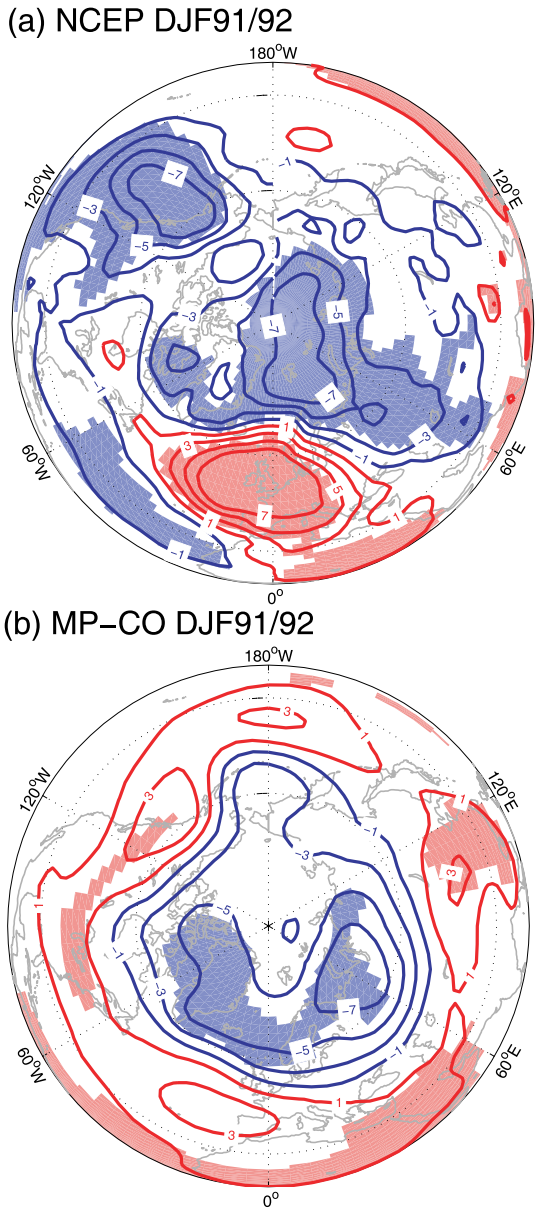

Fig. 6. Winter-averaged (DJF) anomalies of the SLP (hPa) for 1991/92 from the (a) NCEP reanalysis data with respect to the 1985–90 climatology, and (b) the model simulations (MP−CO). The contour interval is 2 hPa. Positive anomalies are shown in red. The shading in (a) corresponds to anomalies larger than one standard deviation, with the standard deviation calculated using winter-mean quantities for the period between 1951–1990, while the shading in (b) corresponds to the 90% confidence level using a local t-test.

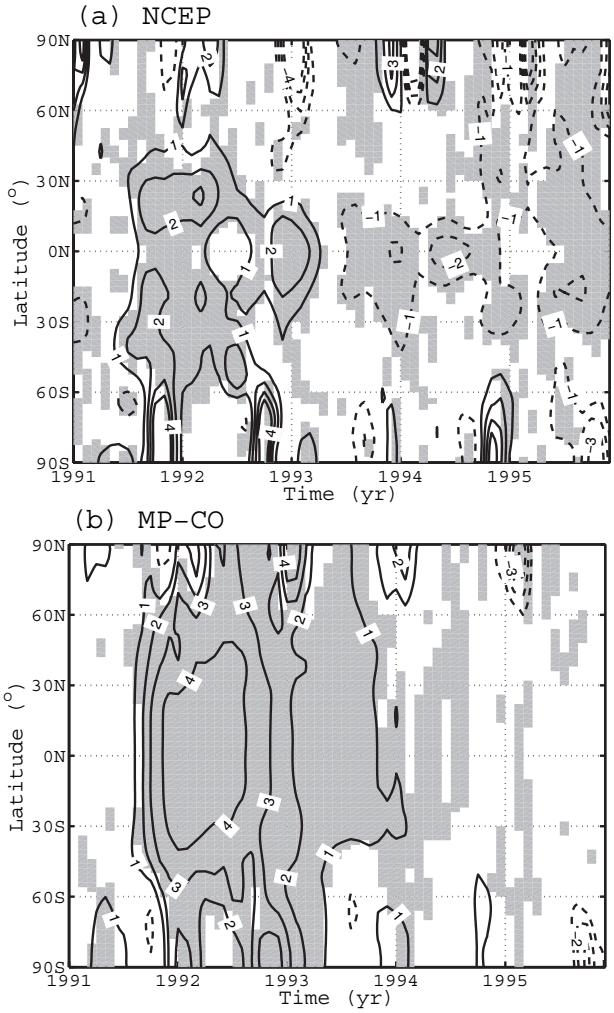

Fig. 7. A Hovmoeller diagram of the zonally-averaged anomalies (K) of the lower stratosphere temperature at the 50 hPa level that were caused by Pinatubo aerosols: (a) calculated from NCEP reanalysis with respect to the 1985–1990 climatology (the shading corresponds to anomalies larger than one standard deviation, with the standard deviation calculated using winter-mean quantities for the period 1951–1990) and (b) the ensemble mean of the model simulations (the shading corresponds to the 90% confidence level).

to the temperature changes in the stratosphere. The heating of the tropical lower stratosphere produced an enhanced Equator-to-pole temperature difference. This in turn, led to an increasing Equator-to-pole geopotential height gradient in the stratosphere (Fig. 9). In the NCEP reanalysis for the winter of 1991/92, the geopotential field at 50 hPa was characterized by strong negative anomalies in the northern polar region and in the eastern part of Russia, and the positive anomalies in excess of 100 m at the mid-latitudes (about 30°–60°N) in North America and Eurasia (Fig. 9a), thus increasing the Equator-to-pole height gradient and strengthening the polar vortex. Although the simulated fields differed to some degree from this pattern (Fig. 9b), it did show a significant deepening of the polar low of the same magnitude as

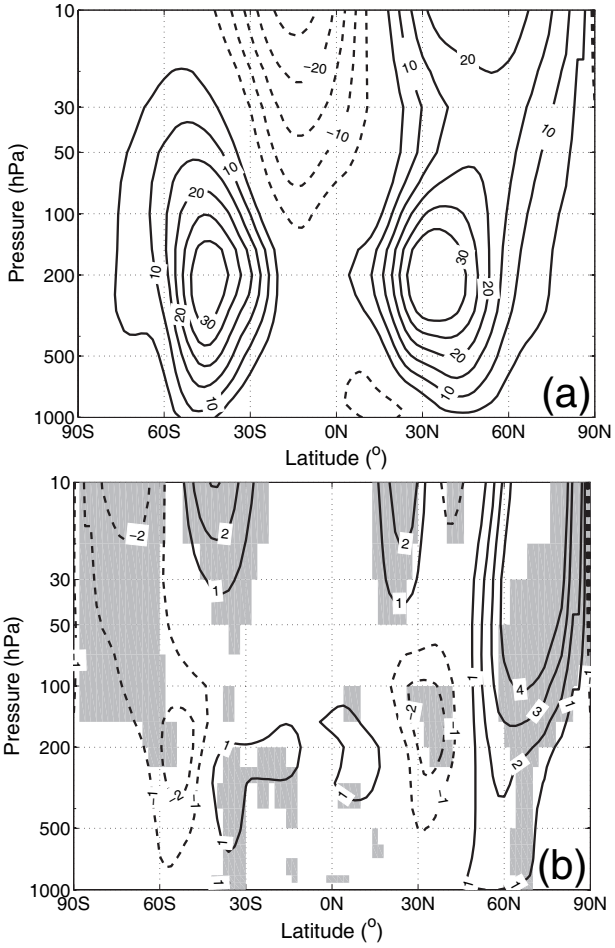

Fig. 8. (a) The zonally-averaged, zonal wind (m s^{-1}) in the CO simulations during winter (DJF). The contour interval is 5 m s^{-1}. (b) The zonally-averaged, zonal-wind anomalies (MP−CO) of the winter of 1991–1992. The shading corresponds to anomalies larger than one standard deviation.

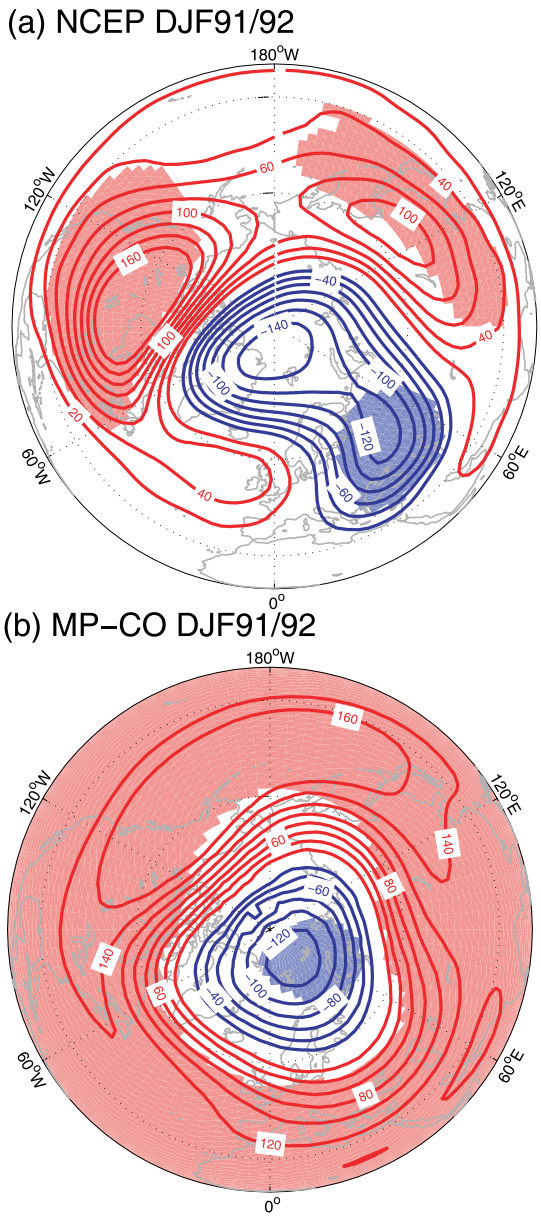

Fig. 9. Winter-averaged (DJF) anomalies in the geopotential height (m) at 50 hPa for 1991/92 from the (a) NCEP reanalysis data with respect to the 1985–1990 climatology, and (b) the model simulations (MP−CO). The contour interval is 20 m. Positive anomalies are shown in red. The shading in (a) corresponds to anomalies larger than one standard deviation, with standard deviation calculated using winter-mean quantities from the period 1951–1990, while the shading in (b) corresponds to the 90% confidence level using a local t-test.

in the observations, and consequently a strengthening of the polar vortex.

To look at the changes in the wave structure in the troposphere, the layer height anomaly at 500 hPa was chosen and was compared with the observations. In the NCEP reanalysis data, the anomaly structure for the winter of 1991/92 was characterized by the negative anomalies over Greenland and the pole, and the positive anomalies in the mid-latitudes over the North Atlantic and Europe, eastern Eurasia and North America (Fig. 10a). In the western portion of the northern hemisphere, the geopotential height anomaly near the Aleutian low that is located over the northeast Pacific was negative, probably being affected by the warm Pacific at this time. The simulated response showed large differences both in the pattern and in the amplitudes of the anomalies observed and simulated (Fig. 10b). The positive anomaly over Great Britain was much weaker than that found in the observations and was shifted to the west, while the negative anomaly over the Urals was not captured at all. Over the North American continent, the simulated positive anomaly

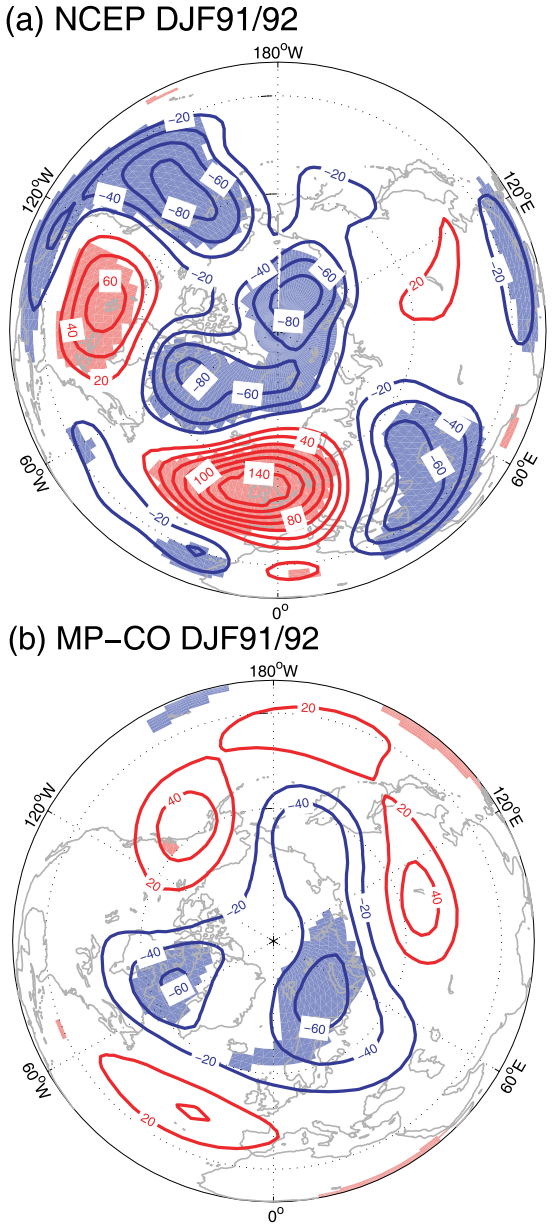

Fig. 10. Winter-averaged (DJF) anomalies of the geopotential height (m) at 500 hPa for 1991/92 from the (a) NCEP reanalysis data with respect to the 1985–1990 climatology, and (b) the model simulations (MP−CO). The contour interval is 20 m. Positive anomalies are shown in red. The shading in (a) corresponds to anomalies larger than one standard deviation, with the standard deviation calculated using winter-mean quantities for the period 1951–1990, while the shading in (b) corresponds to the 90% confidence level using a local t-test.

was located too far northwest when compared to the observations. On the other hand, the negative anomalies found over Greenland and the large parts of the polar region agreed better with the observations.

4. Discussion and conclusions

The present experiments have shown that the atmospheric circulation of the ARPEGE GCM reacts systematically to the imposed volcanic aerosols, and that these simulated changes were similar in many respects to those that were observed after the Mount Pinatubo eruption. It is encouraging that despite the relatively low resolution available in the stratosphere that the model was still capable of simulating many features of the observed climate after the eruption quite well. The model successfully simulated the winter warming over the various landmasses in the NH, although the location of the maximum warming did not agree perfectly with the observations. This winter warming phenomenon was most plausibly explained by a dynamic coupling of the large-scale tropospheric circulation with the state of the stratospheric polar vortex. An anomalously strong and poleward-shifted polar vortex was created (Figs. 8b and 9b), likely as a result of increased Equator-to-pole temperature gradients that were induced by the volcanic aerosol heating. The stronger polar vortex in turn modulated the planetary-wave field in such a way that an anomalously positive AO pattern was produced at the surface including a slightly intensified high pressure anomaly over the North Atlantic (Fig. 6b). Consistent with this pattern were shifts in the Atlantic storm tracks and an increased flow of warm air to Europe and Eurasia, where anomalously high winter SATs were simulated (Fig. 4b).

In addition to the simulated winter-warming phenomenon, the model also reproduced the observed cooling that occured over China in the post-Pinatubo winter quite well. The strong resemblance of the simulation results with the observations during the winter should have been a result of the simulated positive AO/NAO pattern. For instance, recent observational analyses have shown that the cold anomalies that occured over China in cold seasons were related to the NAO (Yu and Zhou, 2004; Li et al., 2005), thereby providing observational evidence supporting the model results.

An alternative explanation for the induced positive-AO pattern was suggested by Stenchikov et al. (2002). They pointed out that *in situ* stratospheric radiative forcing due to aerosols was largely confined to the lower latitudes and therefore did not have a significant, direct effect upon the vortex strength. However, aerosols did have a strong effect on the surface radiative heating and could therefore produce changes in the meridional temperature gradients near the ground, that in turn could affect the large-scale wave fields in the troposphere and in turn the lower stratosphere.

Due to a high signal-to-noise ratio in the tropics, radiatively-induced effects of the volcanic aerosols would most likely have dominated any chaotic dynamic variations in the tropics. However, at higher latitudes the chaotic nature of the winter circulation would likely have played a larger role. It should also be noted that an analysis of the four ensemble members, as performed in this study, was too small to be certain of all aspects of the AO response in the model. Also, one should keep in mind that the real world only went through one realization, and one therefore cannot expect the ensemble mean from the model results presented here to exactly reproduce one particular year.

Another reason for the differences observed between the simulations and the observations was the absence of SST forcing in the simulations. Events such as the El Niños occuring during 1991–1992 and 1993 (Trenberth, 1997) complicate the interpretation of the observed changes. Yang and Schlesinger (2001) performed composite and statistical analyses in an effort to detect and separate the signals of the Pinatubo aerosols and ENSO events in the observed SAT anomalies. They found that the ENSO signals were weak over Eurasia, but relatively strong over the other continents. Over North America, the 1991–1992 El Niño event contributed to more than 50% of the observed total cooling in the summer of 1992. The relatively strong underestimation of the summer cooling over North America in the SAT anomalies (Fig. 5) was therefore likely a result of an ENSO signal in the observed field.

The fact that both SST forcing and Pinatubo aerosols contributed to SAT variations during the target-time period, has also been shown in AGCM simulations. Yang and Schlesinger (2002) showed that the signal of SST forcing was stronger in the troposphere and near the surface than it was in the stratosphere, while the signals from the Pinatubo aerosol forcing was strongest in the lower stratosphere. Only when forced by both the Pinatubo aerosols and the observed SST anomalies, could their AGCM capture the observed cooling that occured over land in the summer of 1992.

The ARPEGE model system presented in this study constitutes the atmospheric portion of the Bergen Climate Model (BCM). This is a state-of-the-art climate model developed at the Bjerknes Centre of Climate Research in Bergen (Furevik et al., 2003), and it is also one of the European climate models participating in the recently published Intergovernmental Panel on Climate Change 4th Assessment Report (IPCC AR4). Recently two multi-model studies on the AO response to different forcings, such as greenhouse gases, tropospheric and volcanic aerosols, were published based on the IPCC AR4 archive (Miller et al., 2006; Stenchikov et al., 2006). The models considered in these studies displayed only limiting success in reproducing the observed changes after major volcanic eruptions. The simulated AO response was generally too weak, and some models did not cause a clear AO response. Notably, the strong anomalously high SLP that was observed over the Atlantic sector (Fig. 6a) was not well reproduced by any of the considered models.

The results presented here, indicate that the ARPEGE model does a reasonable job of simulating the AO response to volcanic aerosol forcing compared to many of the IPCC models, but still has problems that are similar to those found in the other IPCC models. Although a generally positive AO pattern was reproduced, the ARPEGE simulations were not able to fully capture the strong anomalously high SLP that ocuured over the Atlantic sector (Fig. 6b), indicating an AO response that was too weak. Furthermore, there were differences both in the pattern and amplitudes of the geopotential height anomalies that were observed and simulated at the 500 hPa level (Fig. 10) that could point out further model deficiencies. One possibility is that the model may not have sufficiently fine horizontal and vertical resolution to adequately treat the complex stratospheric dynamics and the stratosphere-troposphere dynamical interactions. A more detailed treatment of the aerosol characteristics could also possibly help to improve the simulations.

The too weak AO response that was simulated in many of the IPCC AR4 models, could also be related to the fact that most of them simulated an unrealistically intense polar vortex (Stenchikov et al., 2006). This problem could potentially weaken any wave feedback within the models, and possibly prevent the propagation of the stratospheric signals into the troposphere. Furthermore, Castanheira and Graf (2003) and Walter and Graf (2005) showed that a 20 m s^{-1} zonal wind at 50 hPa at the polar circle provided a good estimate for the transition of the vertical-wave propagation regimes. If the winds were located above that limit, a typical positive AO pattern occurred together with the typical winter warming over Eurasia. Most of the IPCC models considered in Stenchikov et al. (2006) were already close to or above this threshold in the climatological mean (Table 3 in Stenchikov et al., 2006). A strengthening of the zonal winds by the volcanic aerosol effects may therefore have not significantly changed the frequency of the positive AO any further, and this may have possibly contributed to many models underestimating winter warming following large volcanic eruptions.

In the simulations presented here, the polar vortex

was actually determined to be weaker than that which was observed. In the CO simulations, the mean zonal wind at 50 hPa averaged over the latitude belt between 55°–65°N was 16.1 m s^{-1} (Fig. 8a) in comparison to the value of 18.6 m s^{-1} reported in the NCEP reanalysis data for the 1951–1999 time period (not shown). In the MP simulations, there was a strengthening of about 4 m s^{-1} in the zonal winds at 50 hPa at the polar circle (Fig. 8b). This will push the zonal winds at the polar circle slightly above the threshold value of 20 m s^{-1}, and likely induced a positive AO change. This could possibly explain the relatively good resemblance of the ARPEGE simulations with the observations during the winter, when compared to many of the IPCC models. However, the IPCC models were run in coupled mode, while the simulations presented here were run with climatological SSTs in atmosphere-only mode. Also, Stenchikov et al. (2006) based their analysis on the anomaly field composites over several volcanic eruptions, while the results presented here were only influenced by the Mount Pinatubo eruption. It remains to be seen, whether the simulated winter warming pattern can be successfully reproduced when ARPEGE is coupled to an ocean model (e.g., BCM).

It would also be interesting to compare the responses of the model to volcanic aerosol loadings, with other aspects of the model behaviour. Current IPCC AR4 coupled climate models were not able to reproduce the observed trends that occured over recent decades in the AO component of the circulation, and thus did not capture the intensification of the various warming trends that have been observed over Northern Europe and Asia (Miller et al., 2006). It could very well be that current climate models have a basic inadequacy that does not allow for the simulation of a sufficiently strong AO response to large-scale forcing, and that this is also reflected in simulated responses to volcanic aerosols. To address these and other issues, a natural extension of the presented study would therefore be to use BCM to carry out long transient simulations of the last millennium using reliable records of external forcing, such as volcanic eruptions, solar irradiance and greenhouse gases.

The implementation of the volcanic aerosols in ARPEGE simulations presented here, ensures a more realistic simulation of volcanic eruptions for the last millennium when compared to simulations where volcano eruptions were transformed into variations in the solar constant only (e.g., Zorita et al., 2004; Stendel et al., 2006). Despite a relatively low vertical resolution in the stratosphere, the model was able to reproduce many of the observed features that were observed following the Mount Pinatubo eruption, including the winter warming over NH landmasses. This will hopefully help to provide improved simulations of the climate for the past millennium using fully-coupled climate models.

Acknowledgements. The author wishes to thank the two anonymous reviewers for their helpful comments and suggestions that significantly improved this manuscript, and A. Sorteberg and I. K. T. Kindem for useful discussions. Many thanks also to B. J. Soden for kindly providing the ERBS observational data. This study has been supported by the Research Council of Norway through a postdoctoral grant to O.H.O (Project 155957) and by the Program of Supercomputing. This is publication No. A167 from the Bjerknes Centre of Climate Research.

REFERENCES

Angell, J. K., 1997: Stratospheric warming due to Agung, El Chicón, and Pinatubo taking into account the quasi-biennial oscillation. *J. Geophys. Res.*, **102**, 9479–9485.

Briffa, K. R., T. J. Osborn, F. H. Schweingruber, I. C. Harris, P. D. Jones, S. G. Shiyatov, and E. A. Vaganov, 2001: Low-frequency temperature variations from northern tree ring density network. *J. Geophys. Res.*, **106**, 2929–2942.

Castanheira, J. M., and H. F. Graf, 2003: North Pacific-North Atlantic relationships under stratospheric control? *J. Geophys. Res.*, **108**(D1), 4036, doi:10.1029/2002JD002754.

Chen, J., B. E. Carlson, and A. D. D. Genio, 2002: Evidence for strengthening of the tropical general circulation in the 1990s. *Science*, **295**, 838–841.

Chin, M., D. J. Jackob, G. M. Gardner, M. S. Foreman-Fowler, and P. A. Spiro, 1996: A global tridimensional model of tropospheric sulfate. *J. Geophys. Res.*, **101**, 18667–18690.

Crowley, T. J., 2000: Causes of climate change over the past 1000 years. *Science*, **289**, 270–277.

Crowley, T. J., S. K. Baum, K.-Y. Kim, G. C. Hegerl, and W. T. Hyde, 2003: Modeling ocean heat content changes during the last millennium. *Geophys. Res. Lett.*, **30**(18), 1932, doi:10.1029/2003GL017801.

Déqué, M., C. Dreveton, A. Braun, and D. Cariolle, 1994: The ARPEGE/IFS atmosphere model: A contribution to the French community climate modelling. *Climate Dyn.*, **10**, 249–266.

Esper, J., E. R. Cook, and F. H. Scweingruber, 2002: Low-frequency signals in long tree-ring chronologies for reconstructing past temperature variability. *Science*, **295**, 2250–2253.

Furevik, T., M. Bentsen, H. Drange, I. K. T. Kindem, N. G. Kvamstø, and A. Sorteberg, 2003: Description and validation of the Bergen Climate Model: ARPEGE coupled with MICOM. *Climate Dyn.*, **21**, 27–51, doi:10.1007/s00382-003-0317-5.

Groisman, P. Y., 1992: Possible regional climate conse-

quences of the Pinatubo eruption: An empirical approach. *Geophys. Res. Lett.*, **19**, 1603–1606.

Hammer, C. U., B. Clausen Jr., and C. C. Langway Jr., 1997: 50,000 years of recorded volcanism. *Climate Change*, **35**, 1–15.

Hu, R. M., S. Planton, M. Déqué, P. Marquet, and A. Braun, 2001: Why is the climate forcing of sulfate aerosols so uncertain? *Adv. Atmos. Sci.*, **18**, 1103–1120.

Hu, Z. Z., S. Yang, and R. Wu, 2003: Long-term climate variations in China and global warming signals. *J. Geophys. Res.*, **108**(D19), 4614, doi:10.1029/2003JD003651.

Hurrell, J. W., 1995: Decadal trends in the North Atlantic Oscillation: Regional Temperatures and Precipitation. *Science*, **269**, 676–679.

Jones, P. D., and A. Moberg, 2003: Hemispheric and large-scale surface air temperature variations: An extensive revision and an update to 2001. *J. Climate*, **16**, 206–223.

Jones, P. D., and M. E. Mann, 2004: Climate over past millennia. *Rev. Geophys.*, **42**, RG2002, doi:10.1029/2003RG000143.

Jones, P. D., M. New, D. E. Parker, S. Martin, and I. G. Rigor, 1999: Surface air temperature and its variations over the last 150 years. *Rev. Geophys.*, **37**, 173–199.

Kalnay, E., and Coauthors, 1996: The NCEP/NCAR 40-year reanalysis project. *Bull. Amer. Meteor. Soc.*, **77**(3), 437–471.

Kirchner, I., G. L. Stenchikov, H. F. Graf, A. Robock, and J. C. Antuña, 1999: Climate model simulation of winter warming and summer cooling following the 1991 Mount Pinatubo volcanic eruption. *J. Geophys. Res.*, **104**(D16), 19039–19055.

Li, J., R. Yu, T. Zhou, and B. Wang, 2005: Why is there an early Spring cooling shift downstream of the Tibetan Plateau? *J. Climate*, **18**(22), 4660–4668.

Lorenz, E. N., 1968: Climatic determinism. *Meteor. Monogr.*, **8**, 1–3.

Mann, M. E., R. S. Bradley, and M. K. Hughes, 1999: Northern Hemisphere temperatures during the past millennium: Inferences, uncertainties and limitations. *Geophys. Res. Lett.*, **26**, 759–762.

Miller, R. L., G. A. Schmidt, and D. T. Shindell, 2006: Forced annular variations in the 20th century Intergovernmental Panel of Climate Change Fourth Assessment Report models. *J. Geophys. Res.*, **111**, D18101, doi:10.1029/2005JD006323.

Minnis, P., E. F. Harrison, L. L. Stowe, G. G. Gibson, F. M. Denn, D. R. Doeling, and W. L. S. Jr., 1993: Radiative climate forcing by the Mount Pinatubo eruption. *Science*, **259**, 1411–1415.

Parker, D. E., and J. K. L. Brownscombe, 1983: Stratospheric warming following the El Chicón volcanic eruption. *Nature*, **301**, 406–408.

Penner, J. E., C. C. Chuang, and K. Grant, 1998: Climate forcing by carbonaceous and sulfate aerosols. *Climate Dyn.*, **14**, 839–851.

Quiroz, R. S., 1983: The isolation of stratospheric temperature change due to the El Chicón volcanic eruption from non-volcanic signals. *J. Geophys. Res.*, **88**, 6773–6780.

Reynolds, R. W., and T. M. Smith, 1995: A high-resolution global sea-surface temperature climatology. *J. Climate*, **8**, 1571–1583.

Robertson, A., and Coauthors, 2001: Hypothesized climate forcing time series for the last 500 years. *J. Geophys. Res.*, **106**(D14), 14783–14803.

Robock, A., 1983: The dust cloud of the century. *Nature*, **301**, 373–374.

Robock, A., 2000: Volcanic eruptions and climate. *Rev. Geophys.*, **38**, 191–219.

Robock, A., and J. Mao, 1995: The volcanic signal in surface temperature observations. *J. Climate*, **8**, 1086–1103.

Sato, M., J. E. Hansen, M. P. McCormick, and J. B. Pollack, 1993: Stratospheric aerosol optical depths 1850–1990. *J. Geophys. Res.*, **98**(D12), 22987–22994.

Shindell, D. T., G. A. Schmidt, M. E. Mann, and G. Faluvegi, 2004: Dynamic winter climate response to large tropical volcanic eruptions since 1600. *J. Geophys. Res.*, **109**, D05104, doi:10.1029/2003JD004151.

Soden, B. J., R. T. Wetherald, G. L. Stenchikov, and A. Robock, 2002: Global cooling after the eruption of Mount Pinatubo: A test of climate feedback by water vapor. *Science*, **296**, 727–730.

Solomon, S., and Coauthors, 1998: Ozone depletion at mid-latitudes: Coupling of volcanic aerosols and temperature variability to anthropogenic chlorine. *Geophys. Res. Lett.*, **25**, 1871–1874.

Stenchikov, G., I. Kirchner, A. Robock, H. F. Graf, J. C. Antuña, R. G. Grainger, A. Lambert, and L. Thomason, 1998: Radiative forcing from the 1991 Mount Pinatubo volcanic eruption. *J. Geophys. Res.*, **103**, 13837–13857.

Stenchikov, G., A. Robock, V. Ramaswamy, M. D. Schwarzkopf, K. Hamilton, and S. Ramachandran, 2002: Artic Oscillation response to the 1991 Mount Pinatubo eruption: Effects of volcanic aerosols and ozone depletion. *J. Geophys. Res.*, **107**(D24), 4803, doi:10.1029/2002JD002090.

Stenchikov, G., K. Hamilton, R. J. Stouffer, A. Robock, V. Ramaswamy, B. Santer, and H. F. Graf, 2006: Climate impacts of volcanic eruptions in the IPCC AR4 climate models. *J. Geophys. Res.*, **111**, D07107, doi:10.1029/2005JD006286.

Stendel, M., I. A. Mogensen, and J. H. Christensen, 2006: Influence of various forcings on global climate in historical times using a coupled AOGCM. *Climate Dyn.*, **26**, 1–15, doi: 10.1007/s00382-005-0041-4.

Tanre, D., J.-F. Geleyn, and J. M. Slingo, 1984: First results of the introduction of an advanced aerosol-radiation interaction in the ECMWF low resolution global model. *Aerosols and Their Climatic Effects*, H. E. Gerber and A. Deepak, Eds., A. Deepak Publ., Hampton, Virginia, USA, 133–177.

Thompson, D. W. J. and J. M. Wallace, 1998: The Arctic

Oscillation signature in the wintertime geopotential height and temperature fields. *Geophys. Res. Lett.*, **25**, 1297–1300.

Trenberth, K. E., 1997: The definition of El Niño. *Bull. Amer. Meteor. Soc.*, **78**, 2771–2777.

Udisti, R., S. Becagli, E. Castellano, R. Mulvaney, J. Schwander, S. Torcini, and E. Wolff, 2000: Holocene electrical and chemical measurments from the EPICA-Dome C ice core. *Annals of Glaciology*, **30**, 20–26.

Walter, K., and H. F. Graf, 2005: The North Atlantic variability structure, storm tracks, and precipitation depending on the polar vortex strength. *Atmospheric Chemistry and Physics*, **5**, 1–10.

Wielicki, B. A., and Coauthors, 2002: Evidence for large decadal variability in the tropical mean radiative energy budget. *Science*, **295**, 841–844.

WMO-ICSU, 1984: Optical properties for the standard aerosols of the Radiation Commision. Report WCP-55, World Climate Program, World Meteorological Organization and International Council of Scientific Unions, Geneva.

Yang, F., and M. E. Schlesinger, 2001: Identification and separation of Mount Pinatubo and El Niño-Southern Oscuillation land surface temperature anomalies. *J. Geophys. Res.*, **106**(D14), 14757–14770.

Yang, F., and M. E. Schlesinger, 2002: On the surface and atmospheric temperature changes following the 1991 Pinatubo volcanic eruption: A GCM study. *J. Geophys. Res.*, **107**(D8), doi:10.1029/2001JD000373.

Yu, R., and T. Zhou, 2004: Impacts of winter-NAO on March cooling trends over subtropical Eurasia continent in the recent half century. *Geophys. Res. Lett.*, **31**, L12204, doi:10.1029/2004GL019814.

Yu, R., B. Wang, and T. Zhou, 2004: Tropospheric cooling and summer monsoon weakening trend over East Asia. *Geophys. Res. Lett.*, **31**, L22212, doi:10.1029/2004GL021270.

Zorita, E., H. von Storch, F. J. Gonzalez-Rouco, U. Cubasch, J. Lutherbacher, S. Legutke, I. Fischer-Bruns, and U. Schlese, 2004: Simulation of the climate of the last five centuries. *Meteor. Zeitschrift*, **13**(4), 271–289.